Proceedings of the 21st ICSMGE, Vienna, Austria, 14 – 19 June 2026. Pistrol, Adam & Schweiger (eds.)
Published by: ÖGG, Austrian Society for Geomechanics, Salzburg, Austria, ISBN 978-3-9503898-4-5
https://doi.org/10.53243/ICSMGE2026-1793

Effects of soil specific characteristics on site amplifications in the South Iceland Lowland

Elin Asta Olafsdottir, Bjarni Bessason, Sigurdur Erlingsson
Faculty of Civil and Environmental Engineering, University of Iceland, Reykjavik, Iceland, elinasta@hi.is

ABSTRACT: This study aims to evaluate the set of site amplification factors that are defined in the second-generation Eurocode 8 (EC8-2) for soil sites in the South Iceland Lowland that are characterized by thick deposits of normally consolidated basaltic sandy materials. As an initial case study, the present work concentrates on soft sandy soils deposited on the western bank of the Ölfus River. Active- and passive-source surface wave measurements were conducted in the area to evaluate the in-situ shear wave velocity distribution with depth. Resonant Column and Direct Simple Shear testing was used to evaluate the strain-dependent modulus reduction and damping behavior of the Ölfus River sand. Equivalent-linear (EQL) and non-linear (NL) ground response analyses were subsequently used to model the soil site amplification effects for bedrock depths in the range of 10–50 m, assuming different seismic scenarios. Sets of recorded acceleration time histories from earthquakes in the South Iceland region were used as input motions, thus considering the effects of the record-to-record variability on the modelled site response. The predicted amplification behavior in the EQL and NL analyses are compared with the intensity-dependent values of the site amplification factors in EC8-2, thus, contributing to the evaluation of the revised framework for the local seismic and soil site conditions.

KEYWORDS: South Iceland Lowland, ground response analysis, site amplification factors, second-generation Eurocode 8.

1 INTRODUCTION

Iceland is the most seismically active country in Northern Europe with M_w6−7 quakes, mostly associated with strike-slip motion at 5−10 km depth, having repeatedly occurred within two lateral transform zones; the South Iceland Seismic Zone (SISZ) in the lowlands of South Iceland and the Tjörnes Fracture Zone in the north-east (Einarsson, 2008). A series of major earthquakes struck the SISZ in the early 2000s; M_w6.5 and M_w6.4 events in June 2000, followed by an M_w6.3 event in May 2008 (Jónasson et al., 2021). The quakes all damaged buildings and infrastructure in the region and caused rock fall, landslides and liquefaction, but no residential buildings collapsed and no fatalities occurred (Bessason et al., 2022).

The South Iceland Lowland (SIL) is the main agricultural region in the country, with numerous towns, small settlements and farms in the flat terrain. Its geological setting is shaped by a combination of active volcanism and glaciations, making the characteristics of the local soils in many ways unusual in a global sense (Erlingsson, 2019). The soil deposits in the SIL and along the southern coast of Iceland have largely been formed in catastrophic events in the Holocene epoch, e.g., sub-glacial volcanic eruptions that created vast amounts of basaltic tephra and caused major outburst floods. Hence, the most-encountered soils are normally consolidated basaltic granular materials, often loosely compacted due to the rapid sediment build-up, and with highly irregularly shaped grains, intra-particle voids and fractures. However, due to the lack of experimental data on their strain-dependent dynamic behavior, the effects of the soil-specific characteristics have rarely been accounted for in prior studies on site effects.

The second-generation Eurocode 8 [EC8-2] (CEN/TC 250, 2023) includes a new definition of the elastic design spectrum. For outcropping rock conditions and a return period RP, seismic action is defined by two spectral acceleration parameters, $S_{\alpha,RP}$ and $S_{\beta,RP}$. $S_{\alpha,RP}$ is the maximum response spectral acceleration corresponding to the constant acceleration branch of the horizontal elastic design spectrum (5% damping) and $S_{\beta,RP}$ is the spectral acceleration at T_β = 1 s. To account for site amplification effects, EC8-2 defines six standard site categories (A–F) by the depth to seismic bedrock (H_{800}, identified by V_S > 800 m/s) and the corresponding time-averaged V_S ($V_{S,H}$ or $V_{S,30}$ if $H_{800} \geq$ 30 m), and associated intensity-dependent site amplification factors (SAF) F_α and F_β. Based on existing data, granular soil deposits in the SIL are expected to be classified as C to F, with $V_{S,H}$ commonly in the range of 150−350 m/s (Olafsdottir et al., 2024a).

Current work sets out to evaluate the EC8-2 SAF F_α and F_β for areas in the SIL that are characterized by thick deposits of normally consolidated basalt sand and silty sand. Here we present a case study concentrating on the seismic response of soft silty sand deposits on the western bank of the Ölfus River that have been thoroughly characterized by in-situ and laboratory methods as part of prior studies (Olafsdottir et al., 2024b; Fattahi et al., 2025). Equivalent-linear (EQL) and non-linear (NL) ground response analyses are used to model the soil site amplification effects for different hazard scenarios, and shallow and intermediate-thick soil profiles. The predicted response is compared with the intensity-dependent values of the relevant EC8-2 SAF. Thus, initial steps are taken towards evaluating the revised framework of EC8 for prediction of site amplifications for the local seismic and soil site conditions.

2 IN-SITU SOIL SITE CHARACTERIZATION

Surface wave measurements (SWMs), both active-source MASW (Multichannel Analysis of Surface Waves) and single-station microtremor measurements, were conducted at Arnarbæli (63°56'30"N, 21°12'2"W) on the western bank of the Ölfus River, less than 2 km from the western fault rupture of the 2008 M_w6.3 earthquake. The microtremor recordings were analyzed using the MHVSR technique (Microtremor Horizontal-to-Vertical Spectral Ratio) (SESAME, 2004), to evaluate the fundamental site frequency (f_0), and the RayDec method, to assess the R-wave ellipticity (Hobiger et al., 2009). The MASW data were processed using the phase shift method (Park et al., 1998; Olafsdottir et al., 2024b), to retrieve the R-wave dispersion curve. The interval V_S-depth distribution, including the depth of the soil-bedrock interface, was obtained with a joint inversion of the dispersion and ellipticity curves, with the soil stratum modelled as eight layers above a half-space representing bedrock.

Figure 1 presents the results of the SWMs. The MHVSR analysis revealed a primarily unimodal amplification curve with an estimated peak frequency f_0 of 1.77 ± 0.09 Hz (Figure 1a). The R-wave ellipticity, also shown in Figure 1a, is consistent with the MHVSR over the entire analyzed frequency range, suggesting that the recorded wavefield is primarily comprised

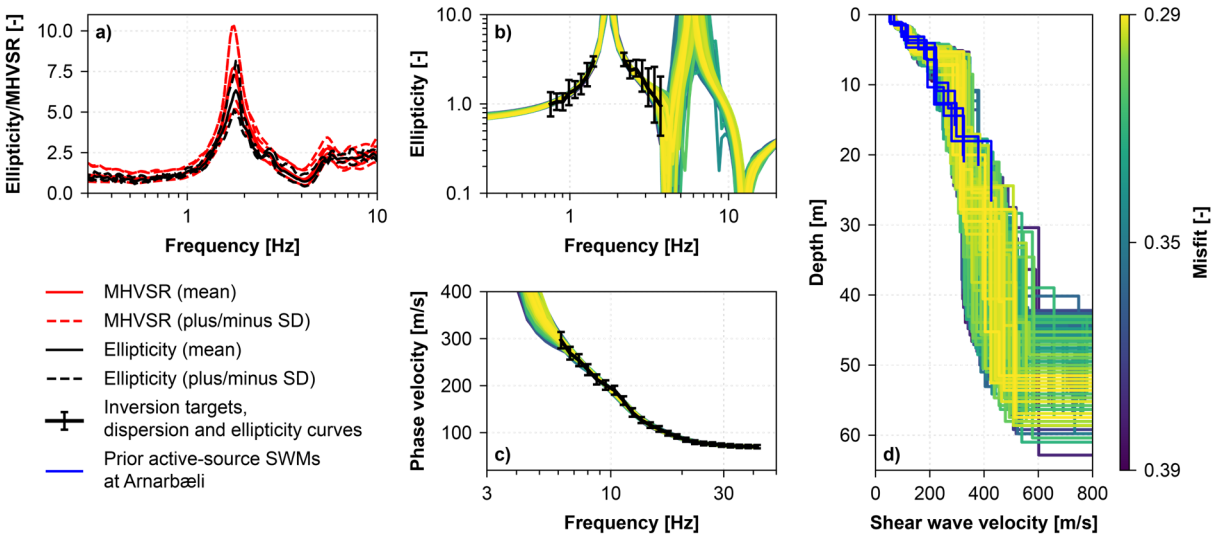

Figure 1. (a) Lognormal median MHVSR and R-wave ellipticity curves for the Arnarbæli site. (b-d) Joint dispersion-ellipticity curve inversion. The set of V_S profiles is color-coded by misfit values, panel (d). The associated theoretically computed dispersion and ellipticity curves are compared to the experimental data points specified as inversion targets in panels (b) and (c).

of R-waves. The set of interval V_S profiles resulting from the joint dispersion and ellipticity curve inversion (Figure 1b-d) indicates a gradual increase in soil V_S with depth, with values ranging from 70 m/s close to surface up to around 400−600 m/s for the deep sediments. This range is consistent with previous active-source SWMs (Figure 1d) conducted in the Arnarbæli area (Olafsdottir et al., 2024b) as well as SWMs conducted at granular soil sites in other low-lying parts of the country (Olafsdottir et al., 2024a). The results in Figure 1d further reveal an abrupt increase in V_S at around 45−58 m depth which is interpreted as depth to underlying bedrock.

3 GROUND RESPONSE ANALYSIS

1-D EQL and NL ground response analyses using RSSeismic (Rockscience, 2025) were used to model the response of the silty sand deposits by the Ölfus River for different seismic scenarios, assuming bedrock depths in the range of 10–50 m.

EQL analysis is simple and computationally efficient and, thus, widely used in geotechnical engineering research and practice. However, at high shear strain (γ) levels, as reached for high-intensity seismic excitations or soft soil profiles like those along the western bank of the Ölfus River, NL analysis methods can provide a more reasonable estimate of the site response (Kaklamanos et al., 2013). However, NL analysis requires a reliable constitutive material model, whose parameters have been carefully calibrated against laboratory data. The required material parameters may not be as well established as the modulus reduction and damping (MRD) relationships required for EQL analysis. The code-to-code variability, associated with the use of different NL numerical schemes, material models and means of model parameter calibration, further adds to the epistemic uncertainty of NL analysis (e.g., Régnier et al., 2018).

3.1 *Velocity profiles*

The median of the interval V_S profiles obtained with the SWMs was used to describe the soil V_S down to a depth of 50 m. To better consider the effects of increased overburden pressure with depth on the V_S distribution, albeit in a simplified manner, a linear increase in V_S was assumed within each of the soil layers. The layer subdivision algorithm in RSSeismic was subsequently used to subdivide each layer with a target frequency of 50 Hz. Four variations of this V_S-depth profile were considered, where the depth to bedrock was specified as $H_{800} \in \{10, 20, 30, 40\}$ m while the sediment V_S was not changed. The resulting set of V_S profiles is shown in Figure 2a. Their EC8-2 site effect proxies are given in Table 1. Following the standard site categorization of EC8-2 (CEN/TC 250, 2023), the profiles are either classified as E (ground class: soft, depth class: shallow) or D (ground class: soft, depth class: intermediate). The bedrock V_S was evaluated as 2,000 m/s which is close to the median value given by the SWMs. The ground water table was assumed at a depth of ~1.5 m.

Table 1. EC8-2 site effect proxies and site categories of the set of V_S profiles used in the EQL and NL analyses.

V_S profile	$V_{S,H}$ (m/s)(*)	H_{800} (m)	EC8-2 site category
P-10	150	10	E
P-20	201	20	E
P-30	234	30	E
P-40	234	40	D
P-50	234	50	D

(*) H = 30 m if $H_{800} \geq 30$ m

3.2 *Strain-dependent material behavior*

Resonant Column (RC) and Direct Simple Shear (DSS) testing was used to evaluate the strain-dependent behavior of the Ölfus River sand, with soil samples retrieved from the location of the SWMs (Figure 2bc). The RC testing was conducted at a mean effective confining pressure (σ'_m) of 100 and 200 kPa. Consistent with existing findings for volcanic-originated sands (Senetakis et al., 2013), the rate of normalized shear modulus (G/G_{max}) degradation and damping (D) increase of the Ölfus River sand was not found to be strongly affected by σ'_m. Likewise, the DSS tests, that were conducted at initial effective vertical stress ($\sigma'_{v,0}$) levels of 100 and 200 kPa (Fattahi et al., 2025), showed that $\sigma'_{v,0}$ had little effect on the reduction of G/G_{max} and on the increase of D at large shear strains. Hence, the MRD behavior of the Ölfus River sand was modelled as independent of depth in the present study. The values of G_{max} for the DSS samples are, however, more uncertain than those of the RC samples. This may lead to a small bias in the large-strain experimental data in Figure 2b, which requires further investigation.

Comparison of literature MRD curves and the element test results revealed that the upper bound G/G_{max} and lower bound

D curves of Seed and Idriss (1970) passably capture the strain-dependent behavior of the Ölfus River sand at low-to-moderate strain levels. However, at larger strains, the upper bound G/G_{max} curve overestimates the DSS-predicted values, with the DSS-results, albeit uncertain, being closer to the lower boundary given by Seed and Idriss. Furthermore, at $\gamma >$ ~0.01%, the lower bound D curve of Seed and Idriss generally predicts slightly larger values than indicated by the RC and DSS tests.

To better describe the dynamic NL behavior of the tested material, the two-parameter G/G_{max}-γ model given by Equation (1) (Roblee & Chiou, 2004) was fitted to the RC data,

$$\frac{G(\gamma)}{G_{max}} = \frac{1}{1 + \left(\gamma/\gamma_{ref}\right)^{a}} \quad (1)$$

where the reference strain (γ_{ref}) and the shape parameter (a) were obtained as γ_{ref}=0.058% and a=1.2. As seen in Figure 2b, the resulting G/G_{max} formulation (red curve) adequately fits the DSS-based values that, due to their higher uncertainty, were not used for the regression analysis.

The damping model described by Equation (2) (Darendelli, 2001; Roblee & Chiou, 2004) was subsequently adjusted to fit the experimental damping values,

$$D(\gamma) = D_{min} + B \cdot D_{masing}(\gamma) \cdot \left(\frac{G}{G_{max}}\right)^{0.1} \quad (2)$$

where the minimum damping ratio at low strains (D_{min}) was obtained as D_{min}=1.2% and the Masing damping (D_{masing}) adjustment factor (B) as B=0.33.

The generalized quadratic/hyperbolic (GQ/H) model with shear strength control (Groholski et al., 2016) was adopted for the EQL and NL analysis. The constitutive model parameters were calibrated to fit the MRD curves for the Ölfus River sand using the reduction factor procedure (MRDF-UIUC) of Phillips and Hashash (2009). It should however be noted that the current MRD estimates of the Ölfus River sand, and by extension the values of γ_{ref}, a, D_{min} and B in Equations (1) and (2), are estimated from a small amount of data where, in particular, the experimental values of D show considerable inter-test scatter. Further measurements are needed to better understand and model the dynamic behavior of the Ölfus River sand, and to better validate the calibrated model parameters.

3.3 *Input motions*

To model the ground response for a range of seismicity levels, five pairs of the EC8-2 spectral acceleration parameters $S_{\alpha,RP}$ and $S_{\beta,RP}$ were used for selection and scaling of the seismic input motions for the EQL and NL analyses. As of late-2025, the seismic hazard in Iceland has not been described in terms of spectral accelerations. Hence, building on the 475-year mean return period reference PGA (a_{gR}) given in the Icelandic National Annexes to EC8 (IST, 2010), i.e., 0.05g–0.5g for the wider South Iceland region and 0.5g for the SISZ, the maximum spectral acceleration was taken as $S_{\alpha,RP} \in \{1.5,3,6,9,12\}$ m/s^2. The corresponding spectral accelerations at T_β = 1 s were estimated as $S_{\beta,RP} = f_h S_{\alpha,RP}$ using the values of f_h defined in EC8-2 (CEN/TC 250, 2023) for the respective seismicity levels.

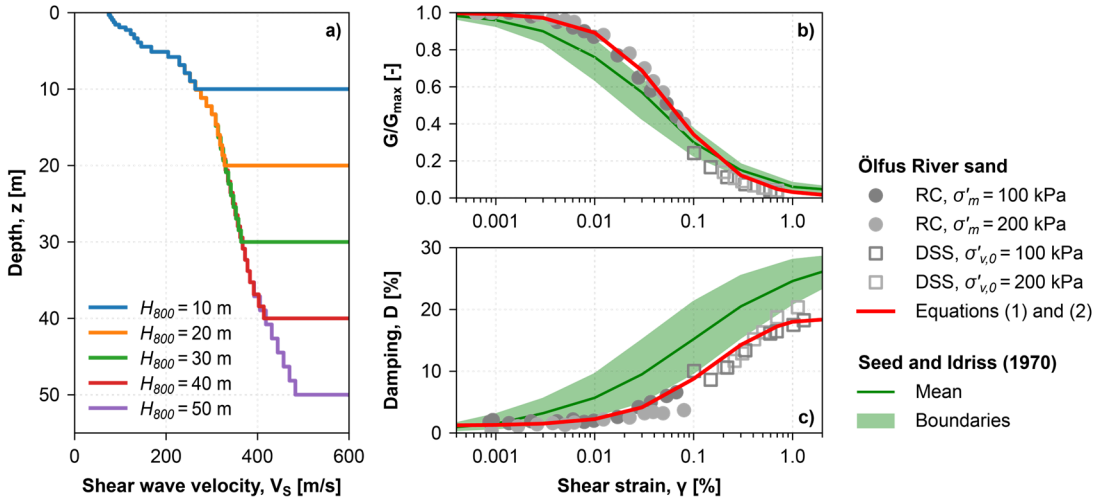

Figure 2. (a) Set of V_S profiles assumed for the EQL and NL ground response analyses. (b, c) Modulus reduction and damping curves.

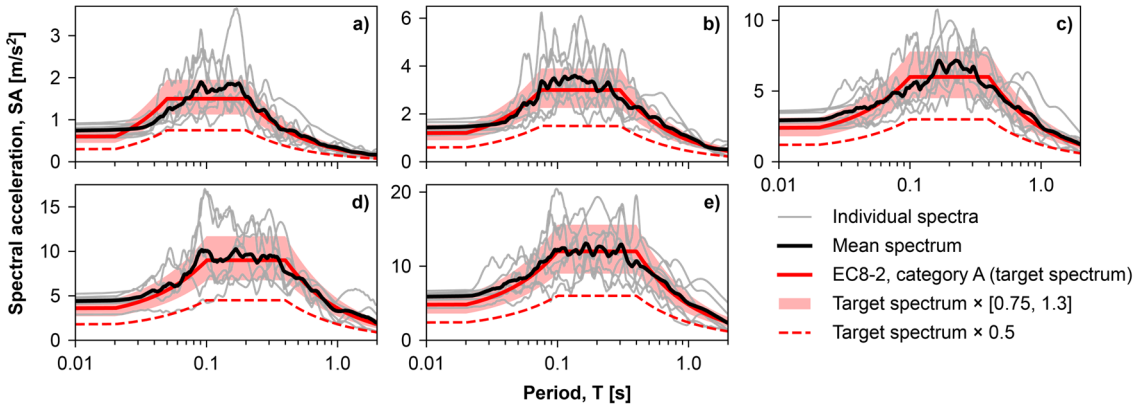

Figure 3. A graphical check of the EC8-2 spectrum compatibility criteria for (a) EQ-class I ($S_{\alpha,RP}$=1.5 m/s^2), (b) EQ-class II ($S_{\alpha,RP}$=3 m/s^2), (c) EQ-class III ($S_{\alpha,RP}$=6 m/s^2), (d) EQ-class IV ($S_{\alpha,RP}$=9 m/s^2), and (e) EQ-class V ($S_{\alpha,RP}$=12 m/s^2).

Five sets of strong ground motions (EQ-classes I to V), recorded at outcropping bedrock in the 2000 and 2008 SISZ quakes (M_w5.4−6.5, main shocks and aftershocks), were scaled to match the respective EC8-2 site category A response spectra following the criteria defined in Annex D (CEN/TC 250, 2023). Adhering to Section 6.6 of EC8-2, each set consists of seven accelerograms. However, due to the limited number of high-PGA motions recorded at rock sites in the SISZ, the set of motions for $S_{\alpha,RP}$ = 12 m/s^2 (EQ-class V) contains three records of the 2008 M_w6.3 event, each recorded at a different strong-motion station. Figure 3 shows the match between the mean and target spectra for the different levels of $S_{\alpha,RP}$.

4 RESULTS AND DISCUSSION

4.1 *EQL and NL assessment of site response*

Figure 4 summarizes, in terms of surface-bedrock amplification ratios (SR; Equation (3)), the results of the EQL and NL analyses for the five classes of input motions (EQ-classes I to V) and the different soil profiles (P-10 to P-50),

$$SR = \frac{SA_{surface}}{SA_{bedrock}} \tag{3}$$

where $SA_{surface}$ and $SA_{bedrock}$ are the acceleration response spectra at surface and that of reference bedrock. Figure 5 shows the corresponding maximum induced shear strain (γ_{max}) with depth. For clarity, only the mean response for each EQ-class and soil profile is shown in Figure 4 and Figure 5.

The model predictions in Figure 4 present a clearly intensity-dependent ground motion amplification behavior for all five soil profiles, with the peak surface-bedrock amplification ratio decreasing and occurring at longer periods with increased level of $S_{\alpha,RP}$. The mean SR for all analysis cases (i.e., the different combinations of the EQ-class and soil profile) indicates amplification of the input motion over the entire period range considered in the analysis, T = 0.04−4 s. The EQL and NL analysis approaches provide, overall, similar results for the lowest intensity input motions; EQ-classes I and II. For these two classes of input motions, the mean values of γ_{max} are at or below 0.1% at all depths (Figure 5) which, based on the findings of Kaklamanos et al. (2013), is a shear strain level where EQL analysis may be expected to provide sufficient results. For the EQ-class III motions, where γ_{max} reaches ~0.4−0.5% in the top-most 5 m, the differences between the mean SR predicted by the EQL and NL analyses become more apparent. The differences between the EQL and NL results further increase for the EQ-class IV and V response, with the EQL analysis generally predicting greater amplification, particularly at short-to-intermediate periods, $T \approx 0.1-1$ s. This tendence of EQL site response analysis to predict a stronger response near the site resonant frequency as compared to NL approaches is well reported (e.g., Kim et al., 2016).

4.2 *Evaluation of EC8-2 site amplification factors*

Figure 6 compares the predicted values of F_α and F_β, as obtained from the EQL and NL analyses respectively, and the values given in EC8-2 (CEN/TC 250, 2023). The present study adopts the period ranges used by Paolucci et al. (2021) for evaluation of the two SAF, i.e.,

$$F_\alpha = \frac{\int_{0.07}^{0.4} SA_{surface}(T)dT}{\int_{0.07}^{0.4} SA_{bedrock}(T)dT} \tag{4}$$

$$F_\beta = \frac{\int_{0.7}^{2.0} SA_{surface}(T)dT}{\int_{0.7}^{2.0} SA_{bedrock}(T)dT} \tag{5}$$

The numerically predicted SAF for each EQ-class (I to V) and soil profile (P-10 to P-50) are represented by the mean and standard deviation of the values obtained for the set of seven input motions (colored error bars in Figure 6). The NL-predicted SAF are given in panels a-d whilst the EQL-based predictions are shown in panels e-h. The EC8-2 values of F_α and F_β for each seismicity level and soil profile, obtained using $V_{S,H}$, H_{800} and the continuous variability SAF expressions introduced in the revised code, are shown with x-shaped markers. Further shown are the default EC8-2 values for site categories D and E (black lines). For a given site category, the default formulae assume a linear relationship between F_α and $S_{\alpha,RP}$, and F_β and $S_{\beta,RP}$, respectively, and are intended for cases where the values of $V_{S,H}$ and H_{800} are not available.

As shown in Figure 6 (panels a, b, e and f), the numerically predicted values of the short-period SAF exceed the values of F_α defined in EC8-2 for all seismicity levels and both the site category D and E soil profiles. The EQL-based values of F_α for EQ-classes III–V ($S_{\alpha,RP} \geq 6$ m/s^2) may overestimate the ground

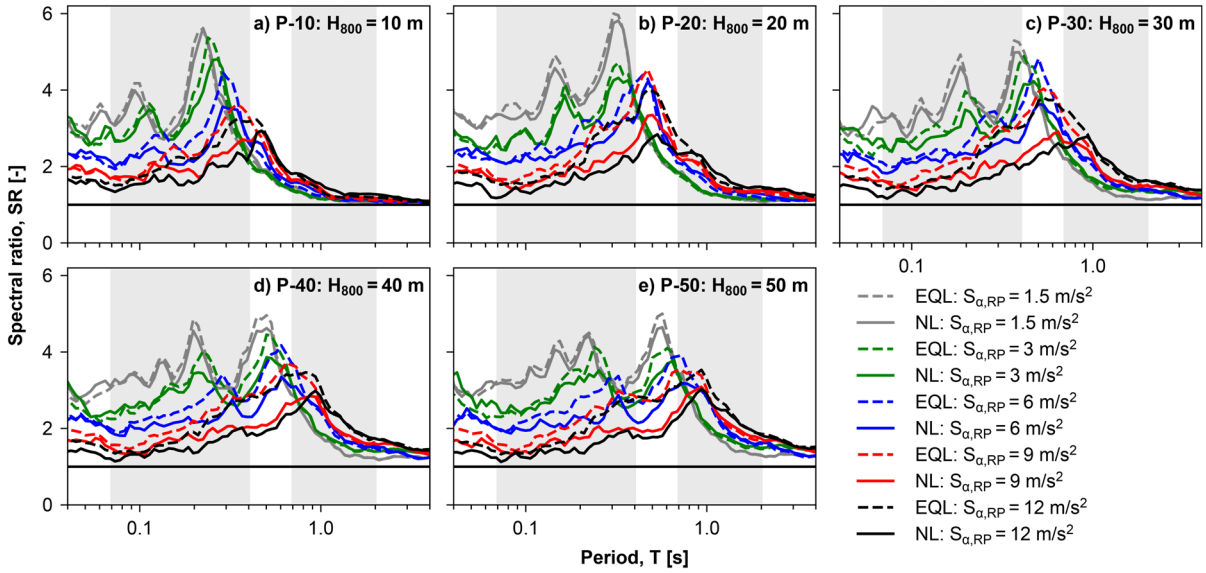

Figure 4. Results of the EQL and NL analyses, given in terms of surface-bedrock amplification ratios, represented by the mean response for each set of input motions. Soil profile (a) P-10 (H_{800} = 10 m), (b) P-20 (H_{800} = 20 m), (c) P-30 (H_{800} = 30 m), (d) P-40 (H_{800} = 40 m), (e) P-50 (H_{800} = 50 m).

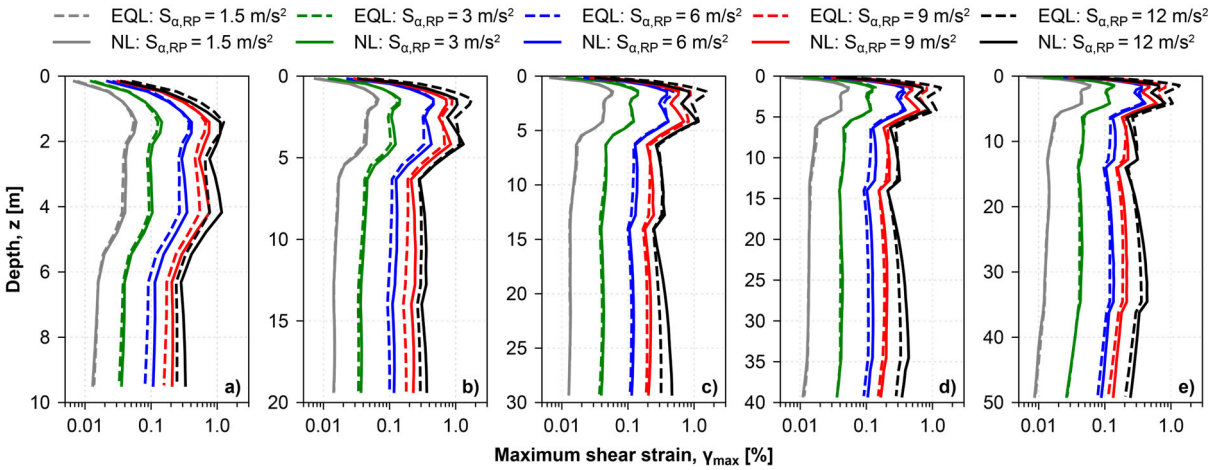

Figure 5. Maximum shear strain profiles resulting from the EQL and NL analyses for soil profiles (a) P-10 (H_{800} = 10 m), (b) P-20 (H_{800} = 20 m), (c) P-30 (H_{800} = 30 m), (d) P-40 (H_{800} = 40 m), and (e) P-50 (H_{800} = 50 m).

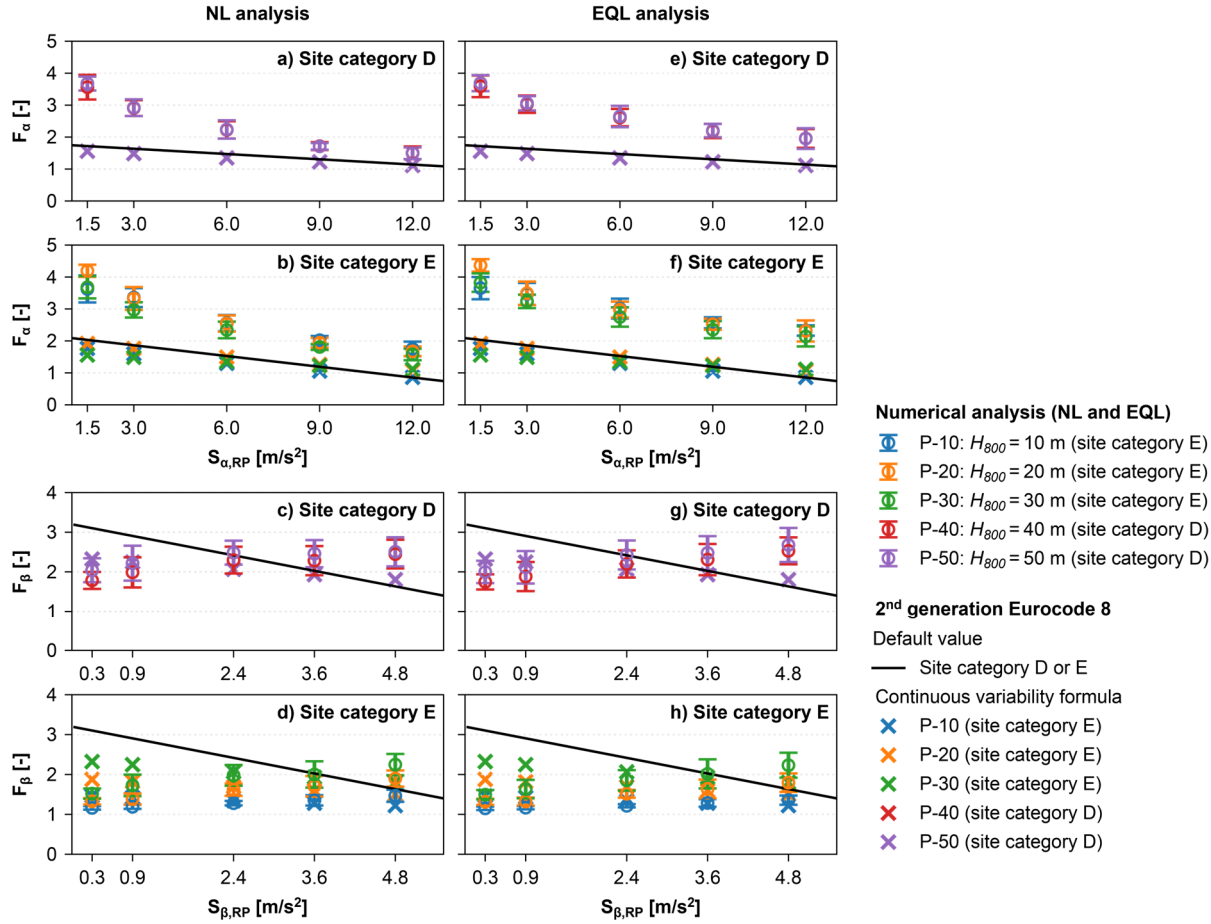

Figure 6. Comparison of numerically predicted values of the short- and intermediate-period amplification factors ($F_α$ and $F_β$) and the values given in the second-generation Eurocode 8 for each soil profile and seismicity level.

motion amplification in the short-period range (Figure 6ef). The NL predictions (Figure 6ab) indicate a larger decrease of $F_α$ with $S_{α,RP}$ as compared to the EQL results. Nevertheless, the mean values of $F_α$ resulting from the NL analysis are 31–114% higher than the default EC8-2 values for the corresponding site category. Considering the continuous-formulated values of $F_α$, these differences increased in most cases.

As can be observed from the bottom-two rows in Figure 6, the intensity-dependence of the EQL- and NL-predicted values of $F_β$ diverts from that assumed by the default $F_β$ formulae for site categories D and E, with the numerical predictions in all cases showing a slight increase in $F_β$ with increased seismicity level. As also indicated by Figure 4, this result of the numerical analyses relates to the predicted elongation of the peak amplification period for successively higher-intensity seismic excitations and the associated shifting of the SR towards higher periods. For EQ-classes I–III (i.e., where $S_{β,RP} \leq 2.4$ m/s²), the numerically predicted values of $F_β$ are generally on the safe side, compared to those given by EC8-2. However, for the higher-intensity input motions and, notably for the category D profiles (Figure 6cg), the mean of the numerically predicted $F_β$ values tend to exceed the values defined by EC8-2.

It should be noted that by assuming $S_{\beta,RP} = f_h S_{\alpha,RP}$, the upper-corner period (T_C) of the EC8-2 response spectrum becomes directly related to the ratio of F_β to F_α. Hence, a high value of F_β (as compared to observed or numerically predicted ground motion amplifications around T_β = 1 s) may be required to prevent insufficiently low values of T_C. This may, e.g., be the case at low-to-moderate seismicity levels for soil profiles showing large short-period amplification, thus requiring high values of F_α to define an appropriate spectrum shape.

5 SUMMARY AND CONCLUDING REMARKS

This work considers the site response of silty sand deposits on the western bank of the Ölfus River in South Iceland. NL and EQL analyses were conducted for five soil profiles, defined using results of SWMs conducted in the area, with assumed bedrock depths of 10–50 m. Five sets of acceleration time histories, each scaled to match the EC8-2 response spectrum (site category A) for a given seismicity level, were used as input motions. The results indicate that the EC8-2 SAF F_α generally underestimate the numerical response of the considered deposits in the short-period range. At intermediate periods and for low-to-moderate seismicity levels, the numerically predicted values of F_β are generally lower than or close to the values given in EC8-2. However, for higher-intensity input motions and the deeper soil deposits, the mean of the numerically predicted F_β values tend to exceed those defined by EC8-2.

As an important step towards better modelling the unusual characteristics of the SISZ volcanic-originated sand in seismic analysis and design, the dynamic material behavior of the Ölfus River sand was determined by RC and DSS tests, thus, providing the initial estimate of MRD curves for SISZ basaltic silty sand. Given the high seismicity in large regions in South Iceland, accurate depiction of the dynamic material behavior is vital for predicting soil site amplifications. In case of NL modelling, the analysis quality is further widely recognized to strongly depend on the selection and calibration of the soil constitutive model. Further work is needed to better understand the capabilities and limitations of different constitutive material models to describe the behavior of the local soils, and to evaluate the effects of the uncertainties in the soil site properties on the modelled response.

It should further be noted that pore water pressure generation was not modelled in the current work. As the Ölfus River sand is known to have liquefied in previous earthquakes, consideration of its potential liquefaction behavior is an important aspect of a comprehensive seismic hazard analysis for the region. The liquefaction behavior of the Ölfus River sand is a subject of ongoing work.

6 ACKNOWLEDGEMENTS

This work was supported by the Energy Research Fund of the National Power Company of Iceland and the University of Iceland Research Fund (grant no. 94242).

7 REFERENCES

Bessason, B., Rupakhety, R., and Bjarnason, J.Ö. 2022. Comparison and modelling of building losses in South Iceland caused by different size earthquakes. *Journal of Building Engineering* 46, 103806

CEN/TC 250. 2023. *EN 1998-1-1:2024. Eurocode 8: Design of structures for earthquake resistance - Part 1-1: General rules and seismic action*. Brussels: CEN.

Darendeli, M.B. 2001. *Development of a New Family of Normalized Modulus Reduction and Material Damping Curves* [PhD dissertation]. Department of Civil, Architectural and Environmental Engineering, The University of Texas, Austin.

Einarsson, P. 2008. Plate boundaries, rifts and transforms in Iceland. *Jökull* 58, 35-58.

Erlingsson, S. 2019. Geotechnical Challenges in Iceland. *Proc. 17th European Conference on Soil Mechanics and Geotechnical Engineering, Reykjavik*, 27-51.

Fattahi, S.J., Jafarian, Y., Konstadinou, M., Olafsdottir, E.A., Erlingsson, S., Bessason, B., and Rupakhety, R. 2025. Liquefaction Behavior of Icelandic Basaltic Sand under Monotonic and Cyclic Direct Simple Shear Loadings. *Geotechnical and Geological Engineering* 43, 531.

Groholski, D.R., Hashash, Y.M.A., Kim, B., Musgrove, M., Harmon J., and Stewart, J.P. 2016. Simplified model for small-strain nonlinearity and strength in 1D seismic site response analysis. *Journal of Geotechnical and Geoenvironmental Engineering* 142(9), 04016042.

Hobiger, M., Bard, P.Y., Cornou, C., and Le Bihan, N. 2009. Single station determination of Rayleigh wave ellipticity by using the random decrement technique (RayDec). *Geophysical Research Letters* 36, L14303.

IST. 2010. *Icelandic National Annexes to Eurocodes*.

Jónasson, K., Bessason, B., Helgadóttir, Á., Einarsson, P., Guðmundsson, G.B., Brandsdóttir, B., Vogfjörd, K.S., and Jónsdóttir, K. 2021. A harmonised instrumental earthquake catalogue for Iceland and the northern Mid-Atlantic Ridge. *Natural Hazards and Earth System Sciences* 21(7), 2197-2214.

Kaklamanos, J., Bradley, B.A., Thompson, E.M., and Baise, L.G. 2013. Critical parameters affecting bias and variability in site-response analyses using KiK-net downhole array data. *Bulletin of the Seismological Society of America* 103(3), 1733-1749.

Kim, B., Hashash, Y.M.A., Stewart, J.P., Rathje, E.M., Harmon, J.A., Musgrove, M.I., Campbell, K.W., and Silva, W.J. 2016. Relative Differences between Nonlinear and Equivalent-Linear 1-D Site Response Analyses. *Earthquake Spectra* 32(3), 1845-1865.

Olafsdottir, E.A., Erlingsson, S., and Bessason, B. 2024a. Database of measured shear wave velocity profiles for Icelandic soil sites. *Proc. 18th European Conference on Soil Mechanics and Geotechnical Engineering*, Lisbon, 3190-3193.

Olafsdottir, E.A., Bessason, B., Erlingsson, S., and Kaynia, A.M. 2024b. A Tool for Processing and Inversion of MASW Data and a Study of Inter-Session Variability of MASW. *Geotechnical Testing Journal* 47(5), 1006-1025.

Paolucci, R., Aimar, M., Ciancimino, A., Dotti, M., Foti, S., Lanzano, G., Mattevi, P., Pacor, F., and Vanini, M. 2021. Checking the site categorization criteria and amplification factors of the 2021 draft of Eurocode 8 Part 1–1. *Bulletin of Earthquake Engineering* 19(11), 4199-4234.

Park, C.B., Miller, R.D., and Xia, J. 1998. Imaging dispersion curves of surface waves on multi-channel record. *SEG technical program expanded abstracts. SEG International Exposition and 68th Annual Meeting*, New Orleans, 1377-1380.

Phillips, C., and Hashash, Y.M.A. 2009. Damping formulation for nonlinear 1D site response analyses. *Soil Dynamics and Earthquake Engineering* 29(7), 1143-1158.

Régnier, J., Bonilla, L.-F., Bard, P.-Y., Bertrand, E., Hollender, F., Kawase, H., Sicilia, D., Arduino, P. et al. 2018. PRENOLIN: International Benchmark on 1D Nonlinear Site-Response Analysis—Validation Phase Exercise. *Bulletin of the Seismological Society of America* 108(2), 876-900.

Roblee, C., and Chiou, B. 2004. A proposed geoindex model for design selection of non-linear properties for site response analysis. *International workshop on uncertainties in nonlinear soil properties and their impact on modeling dynamic soil response*.

Rockscience. 2025. *RSSeismic* (v.1.0). [Software].

Seed, H.B., and Idriss, I.M. 1970. *Soil moduli and damping factors for dynamic response analyses. Report No. EERC 70-10*. Berkeley: Earthquake Engineering Research Center.

Senetakis, K., Anastasiadis, A., and Pitilakis, K. 2013. Normalized shear modulus reduction and damping ratio curves of quartz sand and rhyolitic crushed rock. *Soils and Foundations* 53(6), 879-893.

SESAME. 2004. *Guidelines for the Implementation of the H/V Spectral Ratio Technique on Ambient Vibrations: Measurements, Processing, and Interpretations. SESAME European research project. WP12 – Deliverable D23.12.*